Supporting Information

Zidovska et al. 10.1073/pnas.1220313110

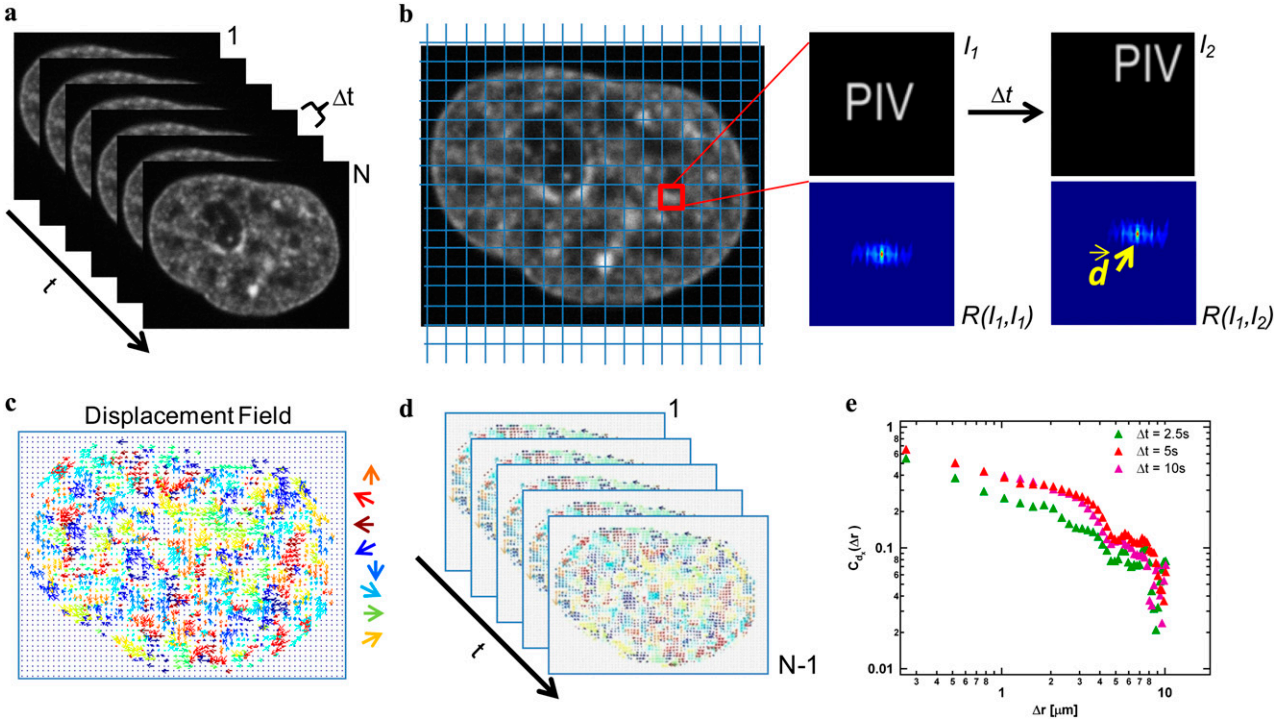

Fig. S1. Schematics of displacement correlation spectroscopy (DCS). (*A*) Using spinning-disk confocal microscopy we record streams of images of nuclei with fluorescently labeled histones H2B-GFP. (*B*) The recorded images are divided into smaller interrogation windows, for each of which an image cross-correlation $R(I_1,I_2)$ is computed between time intervals Δt, using a standard PIV algorithm (1). $R(I_1,I_2)$ directly reports on local chromatin displacement d during Δt in a given interrogation window. (*C*) By computing the displacements d for all interrogation windows, a displacement field for Δt for the entire nucleus is generated. (*D*) Displacement fields are computed for all pairs of images separated by Δt, visualizing the chromatin dynamics as a function of time with temporal resolution Δt. (*E*) The average spatial displacement autocorrelation function (SDACF) $C_{dx}(\Delta r)$ is calculated by averaging over all SDACFs calculated for every displacement field obtained in *D* to detect characteristic length scales. Steps *B*–*E* are repeated for all accessible time lags Δt to obtain temporal evolution of SDACF(Δt), identifying characteristic timescales and length scales in the system.

1. Sveen JK (2004) *An Introduction to MatPIV v. 1.6.1*, eprint series "Mechanics and Applied Mathematics" (Department of Mathematics, University of Oslo, Oslo).

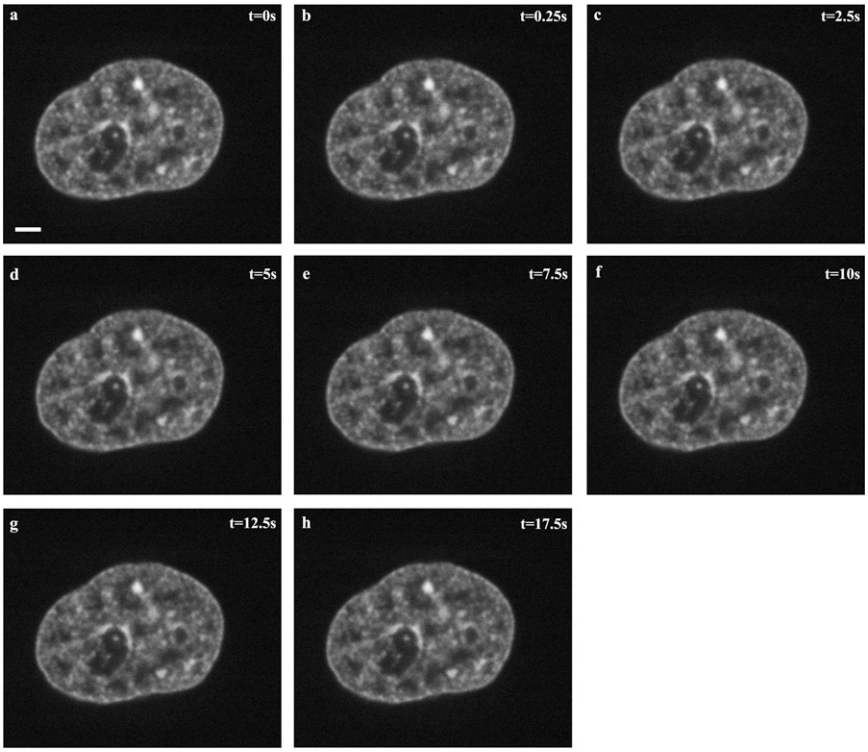

Fig. S2. Confocal microscopy images for Fig. 2. The displacement fields in Fig. 2 were computed from the following pairs of confocal microscopy images: Fig. 2*A*, from *A* and *B*; Fig. 2*B*, from *A* and *C*; Fig. 2*C*, from *A* and *D*; Fig. 2*D*, *Left*, from *A* and *F*; Fig. 2*D*, *Center*, from *C* and *G*; and Fig. 2*D*, *Right*, from *E* and *H*. (Scale bar, 2 μm.)

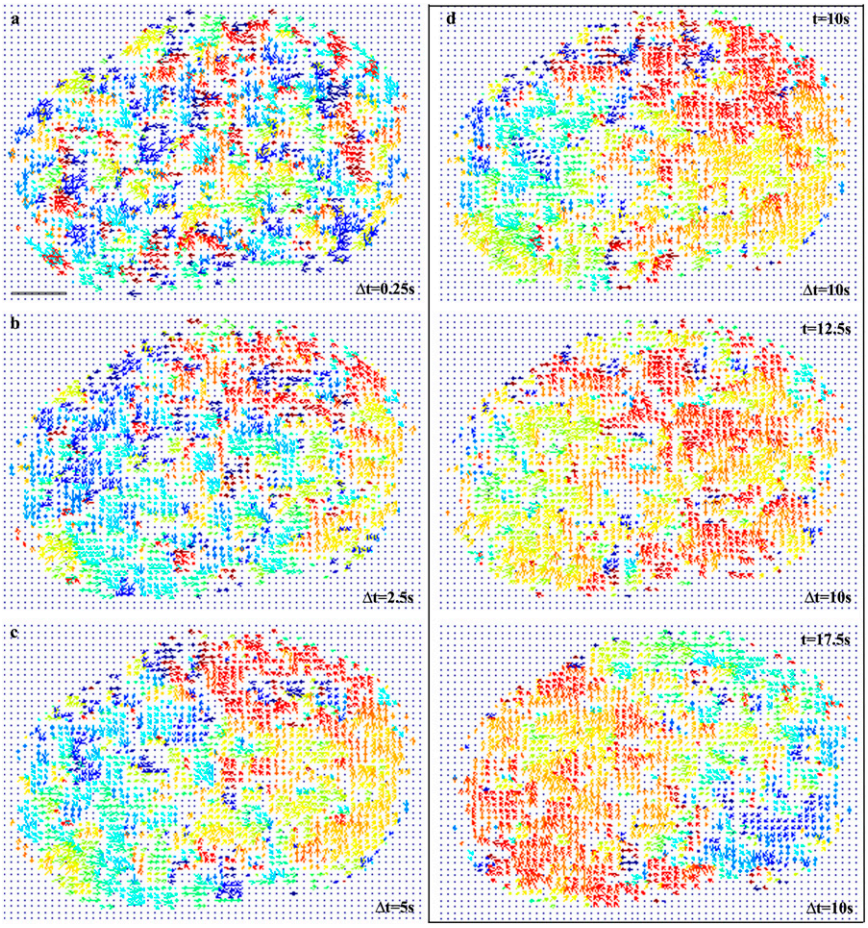

Fig. S3. (*A–D*) High-resolution images of Fig. 2 *A–D*.

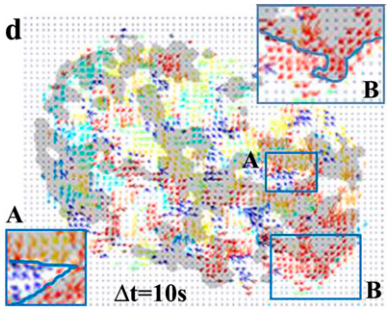

Fig. S4. High-resolution image of Fig. 3*D*. (*A*) An example where boundaries of regions of correlated motion correspond to boundaries between labeled and unlabeled territories. (*B*) An example where regions of correlated motion span across several territories.

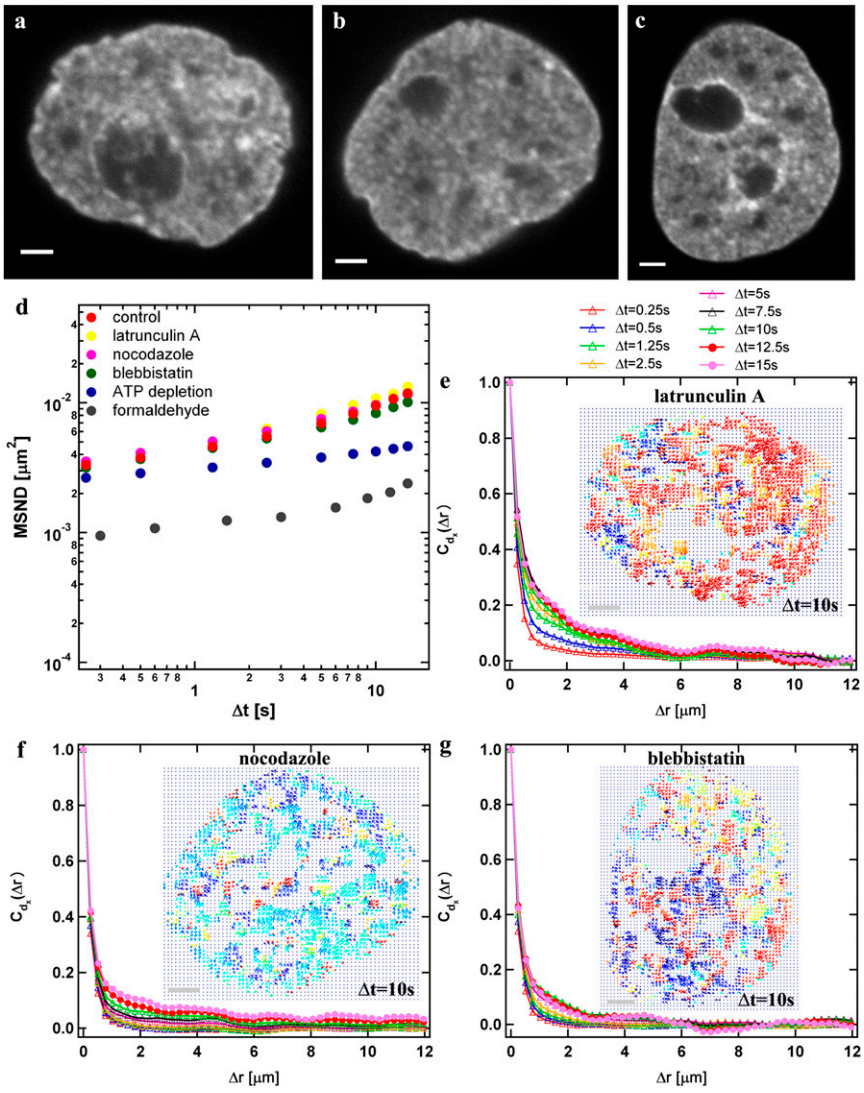

Fig. S5. Cytoskeleton perturbations. We perturbed the cytoskeleton by treating cells with (*A*) latrunculin A, (*B*) nocodazole, and (*C*) blebbistatin. (*D*) Mean square network displacement (MSND) measured for cells treated with latrunculin A ($n = 6$), nocodazole ($n = 8$), or blebbistatin ($n = 6$), respectively, shows that chromatin dynamics persist after the cytoskeleton perturbations and are comparable to the chromatin dynamics under physiological conditions. (*E–G*) We also observe correlated motion after the cytoskeleton was perturbed. (Scale bar, 2 μm.)

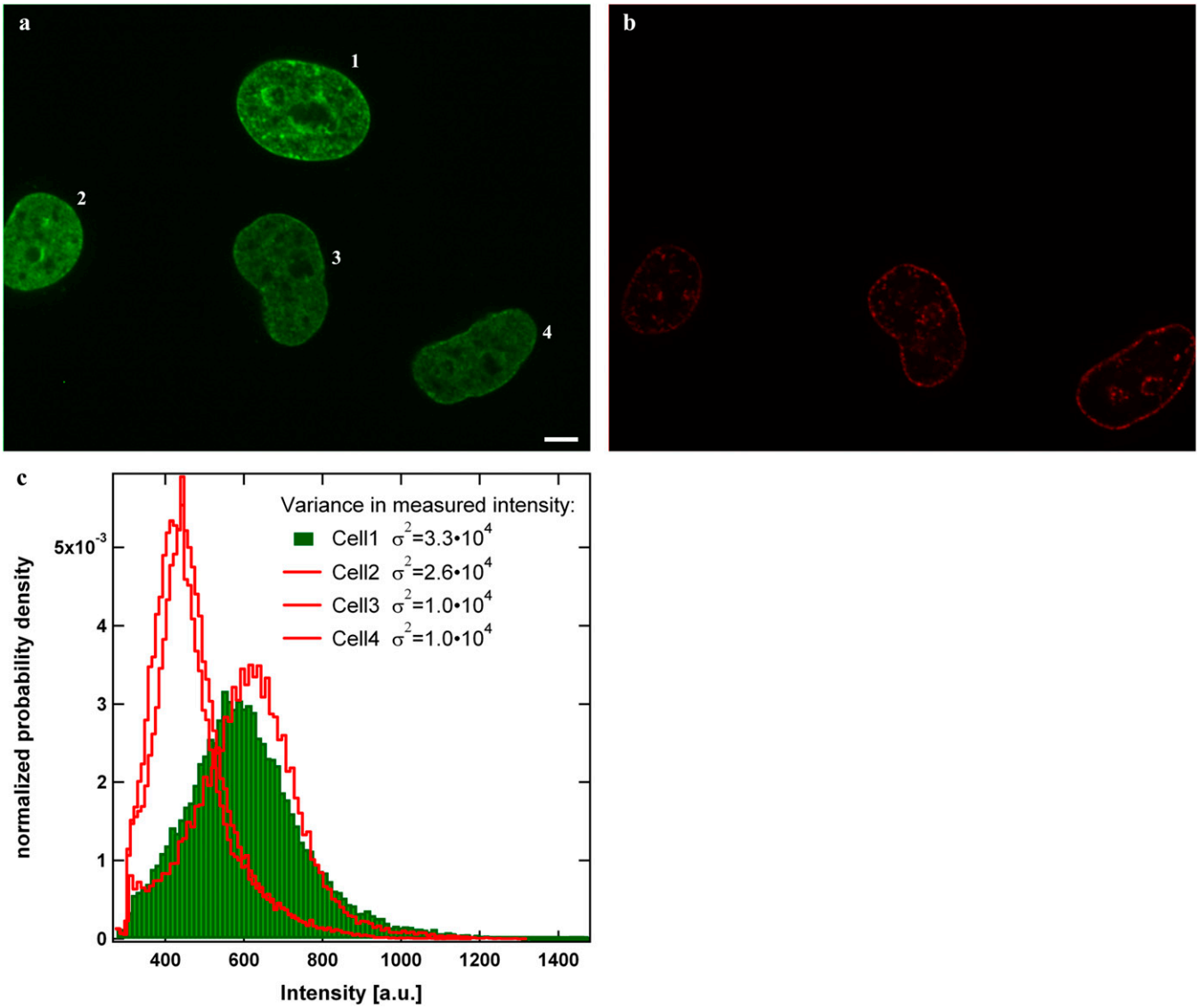

Fig. S6. Aphidicolin's impact is S-phase specific. (*A*) Fluorescent image of four nuclei with histones H2B-GFP (nuclei labelled 1–4 as indicated in the image). (*B*) EdU stain specifically colors (red) only cells in S phase. Nuclei 2–4 show presence of red stain; i.e., they are in S phase. (*C*) Histogram of normalized intensities measured from histone H2B-GFP stain (*A*). Histograms of nuclei 2–4 that are positive for red stain are in red, and the histogram for nucleus 1, which is not in S phase, is shown in green. The variance of measured intensities is lower for nuclei in S phase, suggesting fewer chromatin concentration/density states present. (Scale bar, 5 μm.)

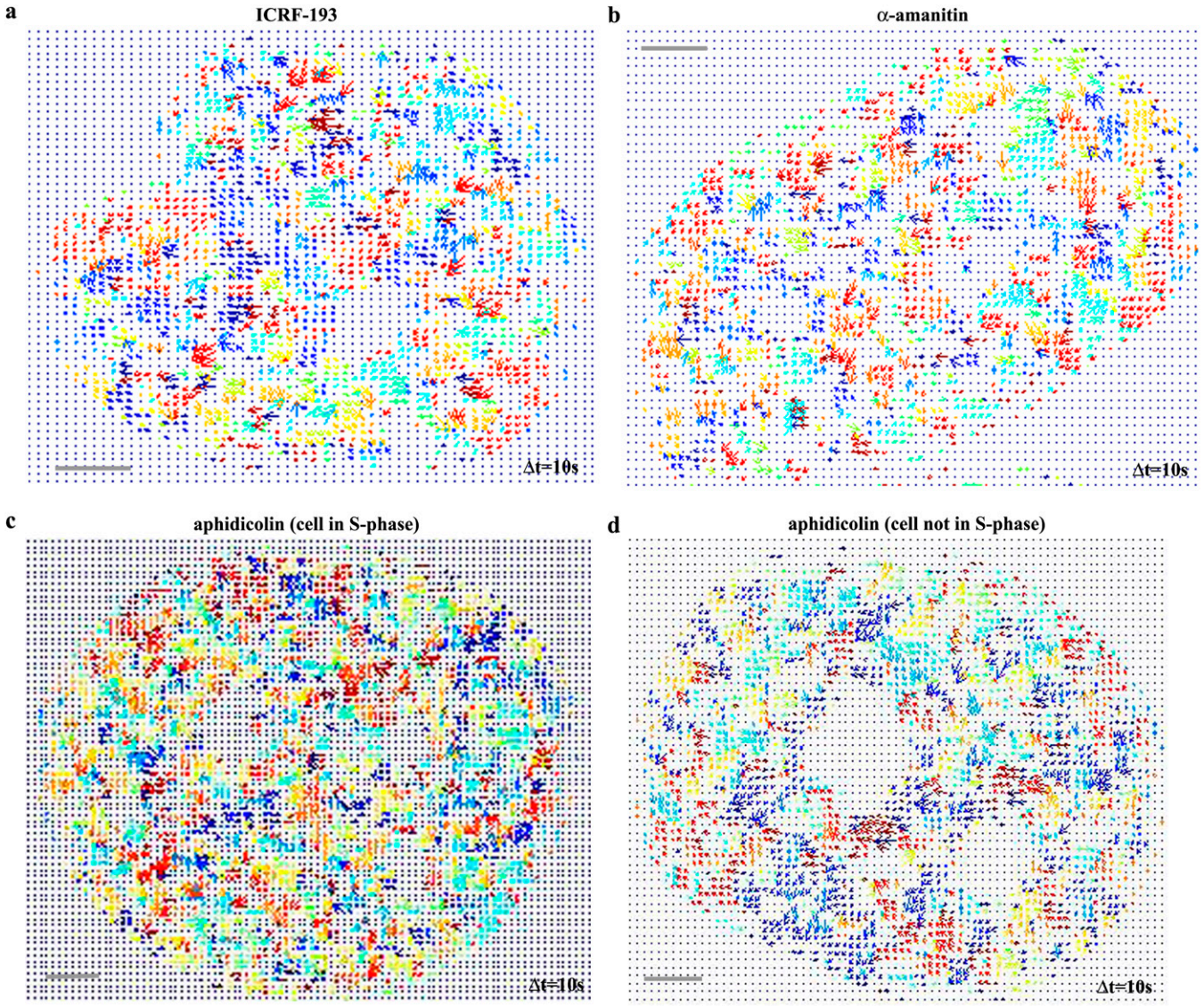

Fig. S7. High-resolution images of Fig. 4 *H–K*. (*A*) Fig. 4*H*; (*B*) Fig. 4*I*; (*C*) Fig. 4*J*; (*D*) Fig. 4*K*.

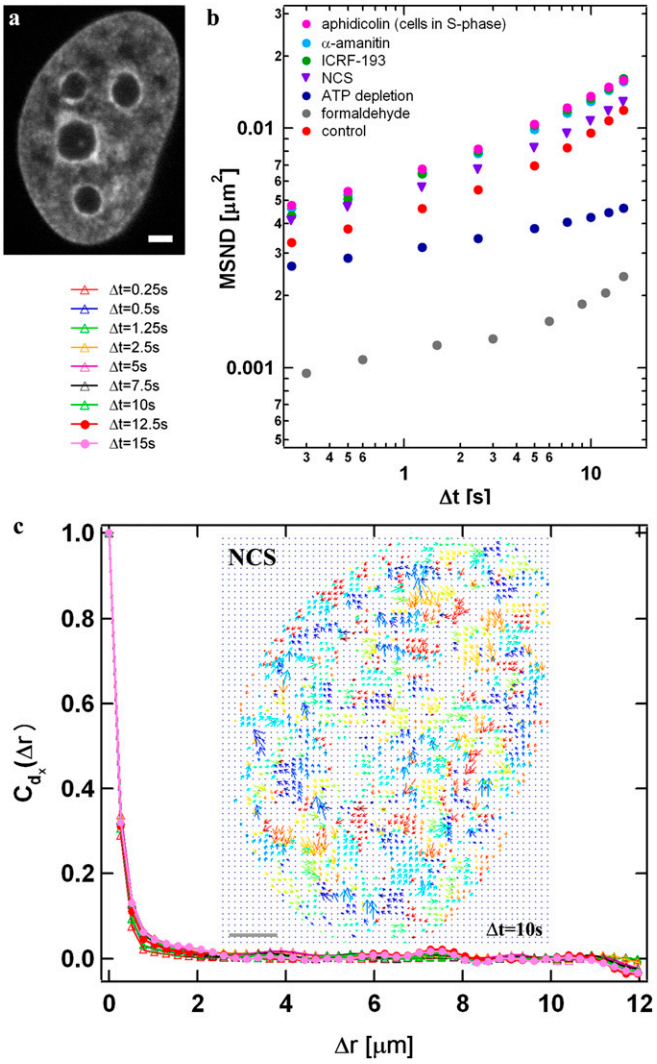

Fig. S8. DNA damage response. (*A*) To investigate chromatin dynamics after direct DNA damage, we treated cells with neocarzinostatin (NCS) that causes DNA double-strand breaks. (*B*) MSND measured for cells treated with NCS (n = 18) shows that local displacements of chromatin increase after direct DNA damage. (*C*) We also find that the local coherent motion is strongly inhibited upon NCS treatment. These observations are consistent with our hypothesis for nuclear enzyme perturbations (Fig. 4); i.e., increase in MSND and loss of local coherence are caused by DNA damage responses induced upon nuclear enzyme perturbations. (Scale bar, 2 μm.)

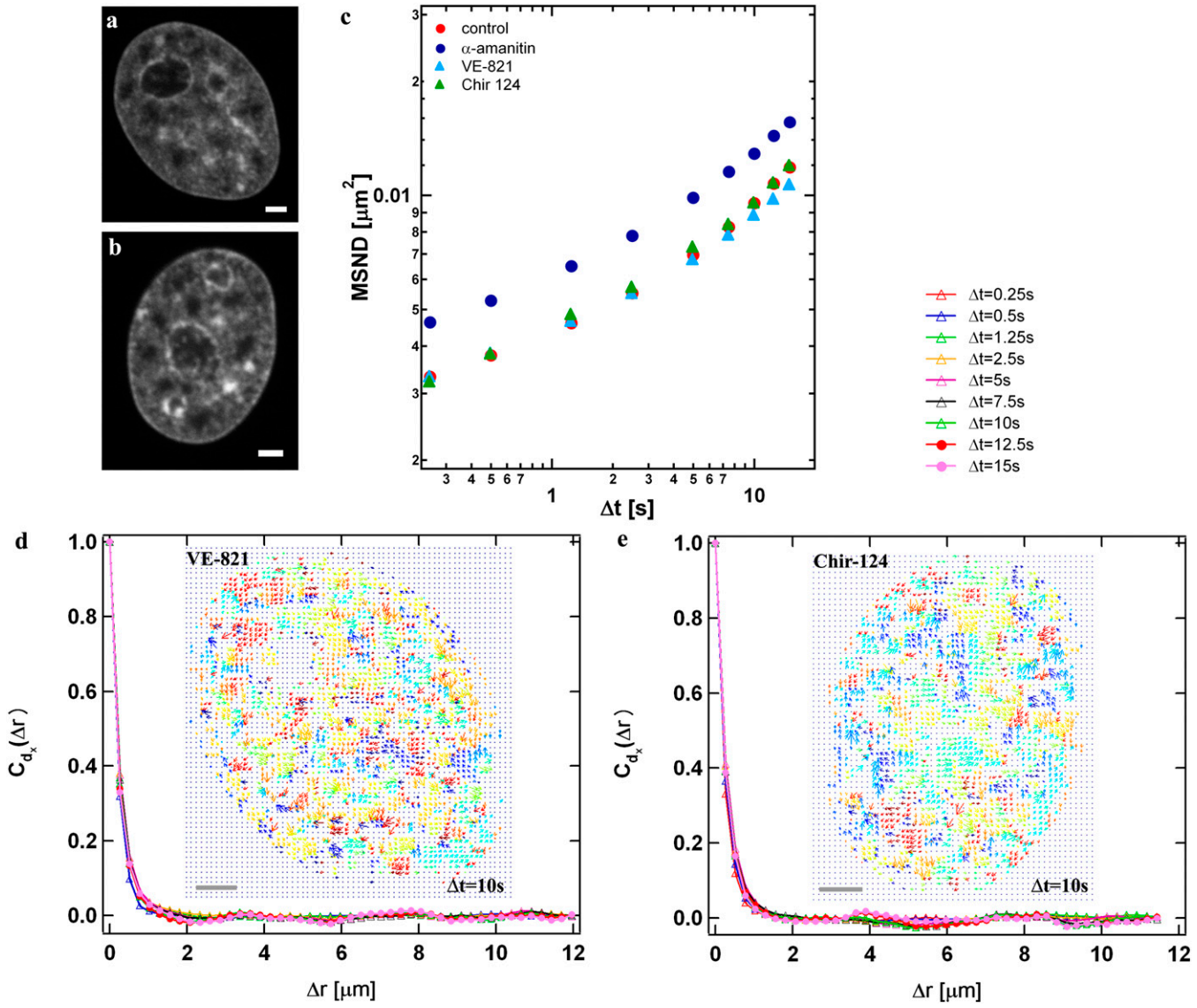

Fig. S9. DNA damage response perturbations. (*A* and *B*) To decouple the contribution of the DNA damage response from the loss of function of the DNA polymerase, RNA polymerase II, and topoisomerase II, we blocked ATR kinase and Chk1 by specific inhibitors (*A*) VE-821 and (*B*) Chir 124, respectively. (*C*) Mean square network displacement (MSND) measured for cells treated with VE-821 (n = 21) or Chir 124 (n = 20), respectively, shows that local displacements of chromatin after perturbing DNA damage responses are comparable with chromatin dynamics under physiological conditions. (*D* and *E*) However, we find that the correlated motion is strongly inhibited after the DNA damage responses were perturbed. These experiments revealed that ATR kinase activity was required for normal dynamics even in unperturbed cells. (Scale bar, 2 μm.)

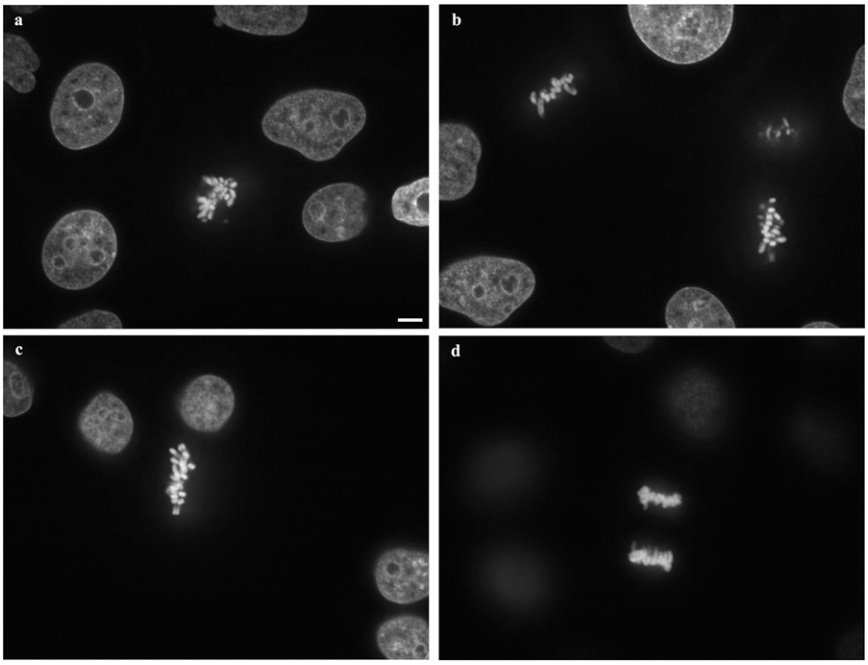

Fig. S10. (*A–D*) Cell viability after DCS measurements. Shown are examples of cells progressing through cell division after DCS measurements. (Scale bar, 5 μm.)